Spatial summation in macaque parietal area 7a follows a winner-take-all rule

Anna Oleksiak, P. Christiaan Klink, Albert Postma, Ineke J. M. van der Ham, Martin J. Lankheet and Richard J. A. van Wezel

J Neurophysiol 105:1150-1158, 2011. First published 22 December 2010; doi:10.1152/jn.00907.2010

Journal of Neurophysiology publishes original articles on the function of the nervous system. It is published 12 times a year (monthly) by the American Physiological Society, 9650 Rockville Pike, Bethesda MD 20814-3991. ISSN: 0022-3077, ESSN: 1522-1598. Visit our website at http://www.the-aps.org/.

J Neurophysiol 105: 1150–1158, 2011.
First published December 22, 2010; doi:10.1152/jn.00907.2010.

Spatial summation in macaque parietal area 7a follows a winner-take-all rule

Anna Oleksiak,[1,2] P. Christiaan Klink,[1,2] Albert Postma,[3] Ineke J. M. van der Ham,[3] Martin J. Lankheet,[4] and Richard J. A. van Wezel[1,2,5]

[1]*Division of Pharmacology, Utrecht Institute for Pharmaceutical Sciences;* [2]*Functional Neurobiology and* [3]*Experimental Psychology, Helmholtz Institute, Utrecht University, Utrecht;* [4]*Wageningen Research Center, Experimental Zoology, Wageningen University, Wageningen; and* [5]*MIRA, Biomedical Signals and Systems Group, University of Twente, Enschede, The Netherlands*

Submitted 20 October 2010; accepted in final form 17 December 2010

Oleksiak A, Klink PC, Postma A, van der Ham IJ, Lankheet MJ, van Wezel RJ. Spatial summation in macaque parietal area 7a follows a winner-take-all rule. *J Neurophysiol* 105: 1150–1158, 2011. First published December 22, 2010; doi:10.1152/jn.00907.2010.— While neurons in posterior parietal cortex have been found to signal the presence of a salient stimulus among multiple items in a display, spatial summation within their receptive field in the absence of an attentional bias has never been investigated. This information, however, is indispensable when one investigates the mechanisms of spatial attention and competition between multiple visual objects. To examine the spatial summation rule in parietal area 7a neurons, we trained rhesus monkeys to fixate on a central cross while two identical stimuli were briefly displayed in a neuron's receptive field. The response to a pair of dots was compared with the responses to the same dots when they were presented individually. The scaling and power parameters of a generalized summation algorithm varied greatly, both across neurons and across combinations of stimulus locations. However, the averaged response of the recorded population of 7a neurons was consistent with a winner-take-all rule for spatial summation. A control experiment where a monkey covertly attended to both stimuli simultaneously suggests that attention introduces additional competition by facilitating the less optimal stimulus. Thus an averaging stage is introduced between ~200 and 300 ms of the response to a pair of stimuli. In short, the summation algorithm over the population of area 7a neurons carries the signature of a winner-take-all operation, with spatial attention possibly influencing the temporal dynamics of stimulus competition, that is the moment that the "winner" takes "victory" over the "loser" stimulus.

vision; parietal cortex; receptive field

IN GENERAL, NEURONAL RESPONSES to multiple, simultaneously presented, high contrast visual stimuli do not simply resemble the sum of the responses to each target in isolation. Although there is a marked heterogeneity, both across and within individual cells, neurons are often classified as either discharging at a rate that approaches the average of responses to individual stimuli (Britten and Heuer 1999; Recanzone et al. 1997; Zoccolan et al. 2005) or at a rate that resembles the highest response obtained with any single target, also known as a winner-take-all (WTA) algorithm (Finn and Ferster 2007; Gawne and Martin 2002; Lampl et al. 2004). Such response normalization has been proposed to result from an increase in the strength and/or number of a neuron's inhibitory inputs (Busse et al. 2009; Ghose and Maunsell 2008; Lee and Maunsell 2009). A similar mechanism is thought to underlie the modulation of single unit responses by attention (Ghose 2009; Reynolds and Heeger 2009). Spatial attention can bias the competition for a neuronal representation between multiple visual stimuli in a cell's receptive field (RF) (Luck et al. 1997; Moran and Desimone 1985; Reynolds et al. 1999) in a way such that when attention is directed towards one of the multiple stimuli, the firing rate of the neuron changes and starts to resemble the response that is usually evoked by the individual presentation of the target stimulus. Crucially, while attention can modulate the gain of specific inputs to a neuron, it does not alter the mechanisms by which a neuron combines the inputs from across its RF but rather acts on top of these mechanisms (Ghose and Maunsell 2008). Consequently, to understand the effects of attention itself, it is important to first determine the fundamental summation rules employed by the neurons under investigation (cf. Ghose 2009; Ghose and Maunsell 2008).

Spatial summation mechanisms have never been investigated in posterior parietal cortex (PPC), an area commonly implicated in controlling spatial attention (Steinmetz and Constantinidis 1995; Gottlieb et al. 1998; Colby and Goldberg 1999; Corbetta and Shulman 2002). For instance, parietal neurons have been shown to express the presence of a behaviorally relevant or perceptually salient stimulus embedded among distracter stimuli (Kusunoki et al. 2000; Constantinidis and Steinmetz 2001, 2005; Bisley and Goldberg 2003, 2006; Ipata et al. 2009). In these studies, the neuronal responses were heavily biased by attention (either bottom-up or top-down) and they are therefore not very informative about the algorithm of unbiased spatial summation. Attentional biases favor a highly nonlinear WTA response mechanism and mask the neuronal representation of the concurrent but unattended stimulus.

In this study, we aimed to determine the elementary spatial summation rule implemented by macaque posterior parietal area 7a neurons under conditions of minimal attentional bias. We recorded from single units while the monkey's attention was directed away from two identical dots in the RF (a fixation task). Responses evoked by a pair of dots were compared with responses to presentations of a single dot at each of the used locations. As a control, we incorporated a delayed match-to-sample task where good performance required attention to be equally distributed over these same two dots. For both experiments, we analyzed the time-averaged response measures as well as at the temporal dynamics of these responses.

METHODS

Subjects and electrophysiological recordings. For all protocols related to animal subjects, we received an approval of the Animal Experiments Review Committee (DEC) of Utrecht University, The

Address for reprint requests and other correspondence: A. Oleksiak, Division of Pharmacology, Utrecht Univ., Sorbonnelaan 16, 3584 CA Utrecht, The Netherlands (e-mail: a.oleksiak.work@gmail.com).

Netherlands. Two male rhesus macaques (*Macaca mulatta*) weighing 8 and 11 kg (monkeys AT and AP, respectively) underwent a surgical procedure to implant a stainless-steal recording chamber and a head post. The recording cylinder was placed over a right (monkey AT) and left (monkey AP) hemisphere craniotomy centered, respectively, at stereotaxic coordinates posterior-lateral of 0.0–11.0 mm and 7.0–14.0 mm relative to the intra-aural line.

Single unit activity was recorded with tungsten microelectrodes (0.1–1.0 MΩ; FHC) manually inserted through a guide tube and further advanced by a hydraulic micropositioner (David Kopf Instruments). Action potentials from single cells were isolated with a window discriminator (BAK Electronics) and registered at a sampling rate of 2 kHz for online analysis and data storage using a Macintosh G4 computer with a National Instruments PCI 1200 data acquisition board.

Postmortem anatomical analysis of the brain tissue confirmed that the recordings in monkey AT were taken from area 7a. Because monkey AP is still participating in another experiment, we do not have histological confirmation of the putative brain region from which the measurements were taken. However, scrupulous mapping and detailed descriptions of all cells that were encountered along the electrode penetration gave us sufficient confidence that we recorded from area 7a. In particular, we were able to establish the course of the intraparietal sulcus (IPS) by charting the grid positions with neuronal activity gaps. The visual cells we recorded from were located in the upper few millimeters of the lateral bank of the IPS and were approached from the medial-anterior positions of the recording chamber. The position of recorded neurons relative to the IPS combined with the fact that the recordings were taken only from the superficial layer (up to ~2 mm from the point of entering gray matter) make a strong case that the site of measurements was indeed area 7a.

Behavioral monitoring. Eye movements were recorded and analyzed online with a video-based eye tracking system (Eyelink II; SR Research) at a sampling rate of 250 Hz in pupil only mode. During an experimental trial, the monkey had to keep its gaze within a virtual window with a radius of 2 deg that was centered on a fixation cross in the middle of the screen. For monkey AT, hand positions were monitored to determine behavioral responses as signaled by raising one of the hands. A 4-cm wide Plexiglas ridge in the primate chair enabled the animal to rest its hands and ensured a standard starting position. Fiber TBV photocells (OMRON E32-DC500), attached 16 mm above the ridge, were connected to an optical fiber photoelectric switch (OMRON E3X-NH) and detected hand movements. This analog signal was amplified, digitized, and sent to the display computer for stimulus control. Visual stimuli were generated using custom-made software running on the same Macintosh G4 computer used for data collection and presented on a 22-in. Sony Graphic Color Display (GDM-500PST), running at a resolution of 1,024 × 768 pixels and a refresh rate of 100 Hz. The experiments took place in a darkened room where the monitor was placed at a distance of 68 cm from the monkey's eyes.

Stimuli and behavioral tasks. Pairs of dots and single dots at one of the two pair locations were presented in a semirandom manner. The fixation cross and stimulus dots were white and subtended, respectively, 0.23 × 0.23 and 0.19 × 0.19 deg of visual angle on a dark grey background. The dots were presented at one or two out of eight equally spaced positions (every 10 deg of arc) along a virtual arc with a radius of 8.9 deg of visual angle centered on the fixation cross (Fig. 1*A*). Due to time limitations, we tested only 10 combinations of pair locations (Fig. 1*B*). These 10 pair locations comprised 4 different distances separating the 2 dots (10, 30, 50, and 70 deg of arc that corresponded with 1.6, 4.6, 7.6, and 10.3 deg of visual angle). This stimulus layout was kept the same across all cells but moved around the perimeter to cover the recorded cell's RF. An example of a one-dot and a two-dot stimulus display is shown in Fig. 1*C*.

From monkey AP, we only required a maintained fixation of the central cross during the stimulus presentation without any behavioral responses. Monkey AT, however, was concurrently trained in another task where similar dot stimuli were relevant for the behavioral performance. To minimize the probability that, in a simple fixation task, monkey AT would still automatically attend to the spatial attributes of the stimulus dots, we incorporated a fixation cross color change that had to be detected and reported by raising the right hand. For both monkeys, a trial began if the gaze was maintained within the central fixation window for 0.4 s. Monkey AT also had to keep its hands in the resting position on the Plexiglas ridge. The following visual stimulation was the same for both animals, with the sample dot(s) being flashed for 0.5 s in the RF of the recorded neuron. After the stimulus offset, a variable duration delay period (0.05–1.0 s) was used with only the fixation cross being visible. For monkey AP, this variable delay was prolonged by 0.9 s and ended with reward delivery. For monkey AT, the variable delay ended with the color change of the central cross (from white to light blue). The behavioral response signaled within 0.6 s terminated this phase of the trial and the final 0.9 s with the reward concluded the whole trial.

Data collection and analysis. The selection of cells and location of the stimulus field were based on neuronal responses to 1-dot presentations at 1 of 12 possible locations spaced every 30 deg of arc on the perimeter of a virtual circle around the fixation cross. This one-dot task allowed a rough estimate of the neuron's RF location. While we placed the stimulus field within the estimated RF, we did not position it exactly at its centre. Rather, the pattern of eight adjacent locations was centered on one of the cardinal or oblique axes, always at the same eccentricity.

We obtained complete recordings of the full set of visual conditions from 24 neurons in monkey AT and from 40 neurons in monkey AP. The median number of trial repetitions per condition (only correct trials) was 13 and 14, respectively, for monkey AT and AP. The data from the two monkeys collected from the fixation task were collapsed (in total 64 neurons) and as such analyzed and illustrated. This procedure is justified by the lack of a significant difference between the two data sets (Wilcoxon rank sum test: $P = 0.32$, z-value = 0.99).

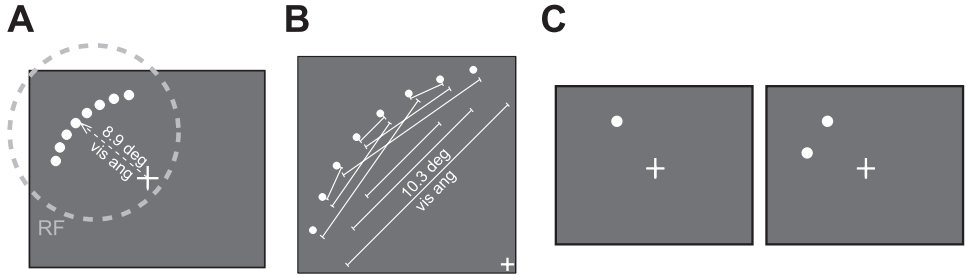

Fig. 1. *A*: stimulus field placed within a neuron's receptive field (RF; grey dashed circle). Dots were flashed individually or in pairs based on specific combinations of the 8 potential single locations. *B*: eccentricity for each recording session was set at 8.9 deg of visual angle. Enlarged stimulus field with lines indicating the 10 pairs of locations used across the whole study. The most externally positioned dots were separated from each other by 10.3 deg of visual angle. *C*: example of a stimulus display (a full screen view) with 1 (*left*) or 2 (*right*) dots placed at locations chosen from the set of 8 positions indicated in *A* and *B*.

For this statistical comparison, we calculated for each neuron a ratio between the mean firing rate elicited by the pair of dots and the average response to the more optimal of the two dots when presented individually (medians for monkey AT and AP were 1.02 and 1.03, respectively).

We examined whether a cell's response to two identical dots that subtended discrete locations within the RF could be predicted by the responses to the individual stimuli. We quantified neuronal responses by calculating average instantaneous firing rate during sample presentation (0.5 s) for each condition (single dot at 8 locations and 10 pairs of dots; Fig. 1, *A* and *B*). In addition to the full data set analyses, we ran the same analyses on a subset of the pairs of dots for which both component dots (locations) elicited a significant response. To classify such dot pairs, a series of paired-sample *t*-tests were run for each neuron and each of the eight dot locations comparing the average firing rate during the 0.5-s sample presentation with the firing rate during a 0.2-s period before stimulus onset ($P < 0.025$, one-sided).

In many analyses we used a classification of the single-dot responses as "max" and "min." These single-dot responses were then compared and the dot location eliciting the higher firing rate was labeled max, whereas the other dot location where response amplitudes were smaller was classified as min. When in the text we refer to pair responses, max-responses, and min-responses, we mean the responses corresponding to the abovementioned definitions.

Spike times were transformed into the standard peristimulus time histograms (PSTHs) with the bins of 10 ms aligned to the stimulus onset. For the population PSTH, we normalized responses for individual cells and each condition before combining it into a grand average. To be specific, the mean responses obtained from averaging across repeats of a condition were normalized to the peak value. For illustrative purposes, the PSTHs for the individual example cells were smoothed with a Gaussian kernel of $\sigma = 10$ ms.

We evaluated a neuron's spatial summation algorithm with a generalized scaled power-law summation (GSP) model that has previously been adopted to explain paired-stimulus responses of macaque MT and V4 neurons (Britten and Heuer 1999; Ghose and Maunsell 2008) but originally developed by Simoncelli and Heeger (1998) to describe the extraction and representation of visual motion. *Equation 1* relates the neuronal response to a pair of stimuli ($RATE_{pair}$) to responses obtained with constituent stimuli, one of which is more optimal then the other ($RATE_{max}$ and $RATE_{min}$):

$$RATE_{pair} = \alpha(RATE_{max}^{n} + RATE_{min}^{n})^{1/n}$$

This equation captures a large range of spatial summation behaviors, including averaging (AVR: $\alpha = 0.5$ and $n = 1$) and WTA operations ($\alpha = 1$, large n). The fitting procedure was executed with the Matlab function *nlinfit* that implements a Gauss-Newton algorithm with Levenberg-Marquardt modifications for global convergence to find least-squares parameter estimates. The percentage of variance accounted for by the model was calculated as 100 * [1 − variance$_{(observed-predicted)}$/variance$_{(observed)}$] (Carandini et al. 1997; Britten and Heuer 1999).

RESULTS

Time-averaged pair responses. Figure 2 illustrates responses of two example neurons (*A* and *B*) to individual dots and to pairs of dots. *Left* represents *top left* quadrant of the display with eight isoeccentric positions at which a single dot appeared while the monkeys fixated a central cross (here indicated at *bottom right*). The mean responses elicited by these individually presented dots are shown at the *bottom* (labeled from 1 to 8, grey line). The black lines on the *right* indicate mean responses to 2 simultaneously displayed dots placed at 10 different pair combinations of the basic 8 positions. For each

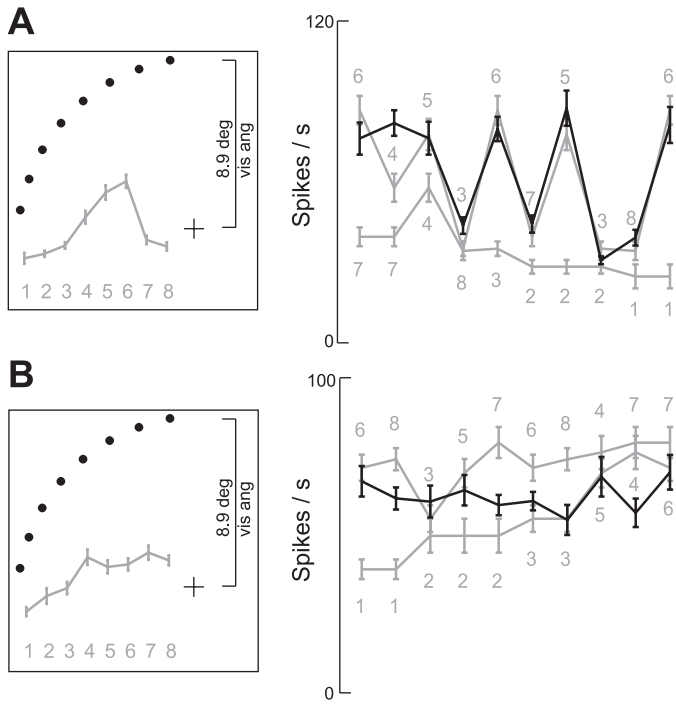

Fig. 2. *A* and *B*: responses of example cells to a single dot and pairs of dots. *Left*: *top left* quadrant of a video display with a single dot presented at 8 locations with an eccentricity of 8.9 deg of visual angle. Cross at *bottom right* indicates the monkey's gaze position during the stimulus presentation. Grey line below indicates the mean firing rate elicited by a single dot flashed at the corresponding locations (labeled 1 to 8). Black lines at *right* show mean responses to the 10 pairs of dots. Grey lines represent mean responses to the individually presented dots (the grey digits indicate the locations from the *left*), sorted to correspond with the dot locations of each pair. These single locations were classified as more responsive and less responsive for each dot pair and plotted as *top* and *bottom* grey lines, respectively. Error bars denote SE across repeats. Connecting lines at *right* are used only for visual guidance.

dot pair, single-dot responses on the constituent locations were classified as more responsive and less responsive and replotted in the graphs on the *right* as the *top* and the *bottom* grey lines, respectively. The corresponding grey digits refer to the locations on the *left*. Figure 2*A* shows the case where the neuron's response to a pair is very similar to the better of the two constituent locations: a WTA rule (the black line overlaps with the *top* grey line). A more variable behavior is shown in Fig. 2*B* where the cell's response to a pair of dots relative to the individual stimulations depends on the particular dot pair. These pair responses show the following behaviors: a WTA algorithm (the black line overlaps with the *top* grey line), a strong inhibitory interaction (the black line overlaps with the *bottom* grey line), and an AVR algorithm (the black line lies between the grey lines).

Temporal dynamics of pair responses. The temporal profile of the responses of the same example neurons is depicted in Fig. 3, *A* and *B*. The mean responses from 10 pair conditions and the corresponding single-dot conditions are plotted as PSTHs for illustrative purposes smoothed with a Gaussian kernel of $\sigma = 10$ ms. *Insets* represent the *top right* quadrant of a video display with a fixation cross in the *bottom right* corner and the positions of the two sample dots. The black lines denote the firing pattern in the pair condition, and the grey lines denote the responses to the component dots. Figure 3*C* summarizes the temporal profile of the population ($n = 64$)

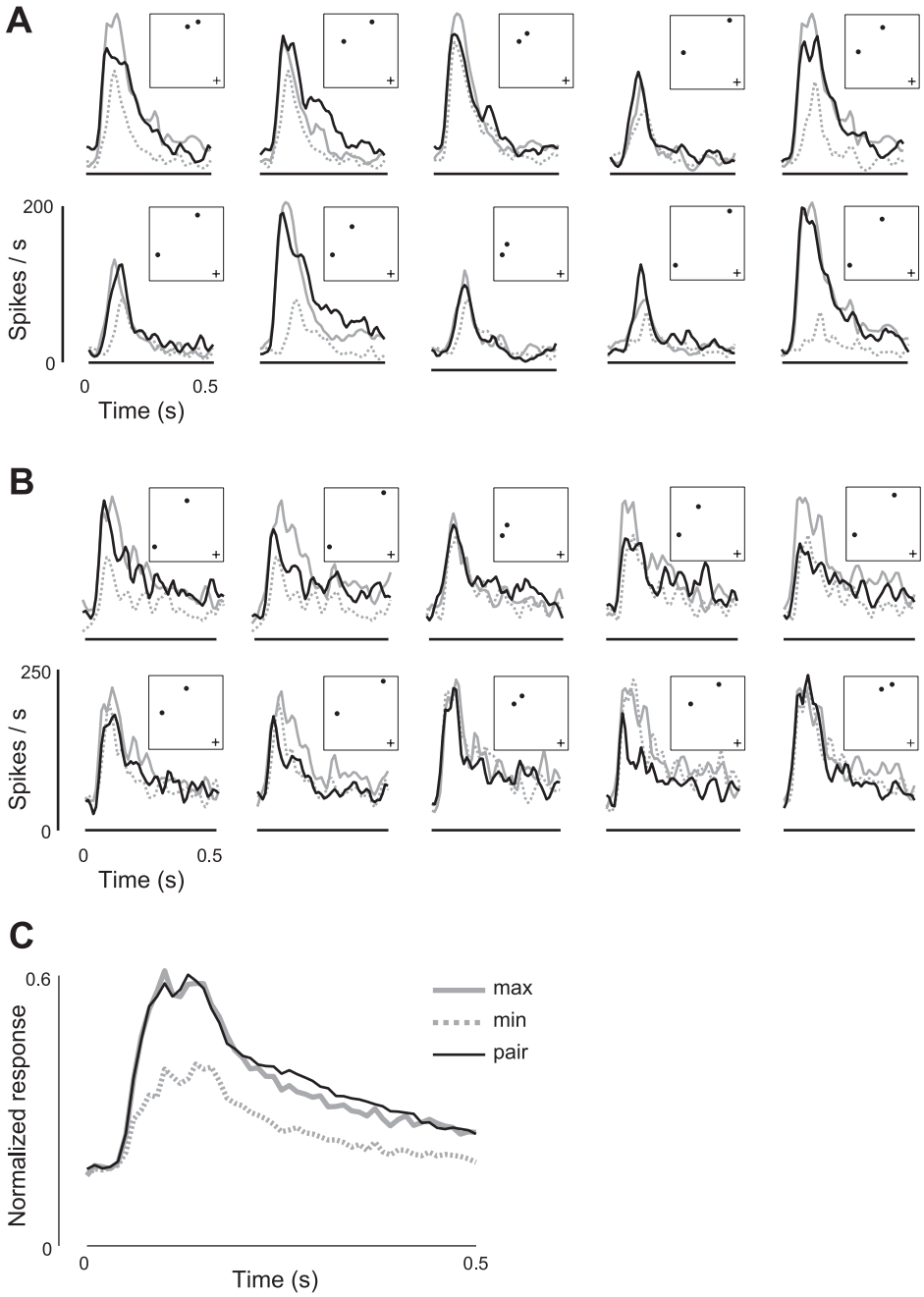

Fig. 3. *A* and *B*: peristimulus time histograms (PSTHs) of 2 example neurons (as in Fig. 2, *A* and *B*) for 10 dot pairs and the corresponding single-dot responses. For these plots, the mean PSTHs were smoothed with a Gaussian kernel of $\sigma = 10$ ms. *Insets*: *top left* quadrant of a video display with the 2 eccentrically flashed dots and a central fixation cross (here in the *bottom right* corner). Black lines denote the dot pair responses, and the grey lines denote the corresponding single-dot responses. *C*: unsmoothed population PSTH ($n = 64$) with normalized responses. Conventions are the same as in *A* and *B*.

response the paired (black line)-dot and single-dot (grey lines) presentations. Before the data were collapsed across conditions and neurons, the PSTHs were normalized and the two dot locations composing a pair were labeled as max and min depending on their relative time-averaged firing rate (higher and lower response, respectively). From this population of PSTH, it is apparent that the dot pairs elicit responses that are very similar in amplitude and across time to the responses evoked by the stimulation of the most responsive of the two component locations (the black pair line overlaps with the solid grey max line).

Based on the time-averaged firing rates, we calculated the best fitting parameters of the GSP model (see *Eq. 1* in METHODS). The best fit to the averaged responses of all recorded single units ($n = 64$) explains 95% of the variance. Importantly, the best-fit scaling parameter α is very close to 1 and the power term n is >1, indicating a highly nonlinear WTA summation algorithm [α-parameter: 1.00, 95% confidence interval (CI) 0.98, 1.03; n-parameter: 18, 95% CI -28, 63]. Very similar results with 97% of explained variance were obtained for a subpopulation of 20 neurons for which all 8 tested single locations evoked a significant "ON" response (α-parameter: 0.97, 95% CI 0.71, 1.22; n-parameter: 9, 95% CI -32, 49). The time-averaged population results are thus in accordance with what can be seen from PSTHs (Fig. 3*C*). However, for individual neurons, only for 38 out of 64 units could the best fitting GSP model explain $>40\%$ of the variance (Fig. 4*A*). Across these neurons, the median parameter α was also close to one ($\alpha = 0.97$) and the median exponent was larger than one ($n = 4$; Fig. 4, *B* and *C*). From these units, the subgroup ($n = 9$) with all tested locations

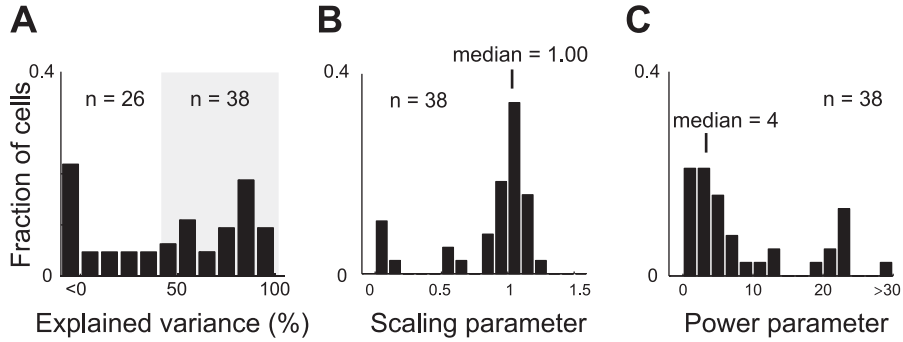

Fig. 4. Generalized scaled power-law summation (GSP) model fits. *A*: results of model fitting for 64 neurons expressed as the percentage of the explained variance accounted for by the model. *B*: distribution of the best-fit scaling parameter α from single units with the best model explaining ≥40% of the pair-response variance ($n = 38$). *C*: same as in *B* but for the power parameter n.

eliciting a significant stimulus response, the median parameter α reached 0.92 and the exponent of 3.

Overall, the results of the model fits demonstrate a number of important issues. The GSP model provides a good description of the summation rule that is operative in the recorded population of area 7a neurons. The average pair responses of the population showed very little scaling and a considerable nonlinearity (but see the CIs of parameter n). However, the model fitting was unreliable for ~40% of the recorded units and even the remaining 38 individual cells yielded median parameter values indicative of a virtual absence of scaling and a nonlinearity of the pair responses that is weak at best. The relatively small number of neurons for which model could be well fit as well as the wide range of parameter values (especially the variability in the power term) might result from a low signal-to-noise ratio at the level of single neurons or the presence of pair responses with large differences in the sensitivity to each of the paired locations.

Figure 5 illustrates the between- and within-neuron variability of responses that likely contributes to the low explanatory power of the model for a number of individual cells. The data in Fig. 5 are plotted in relation to the WTA and AVR summation algorithms that correspond to distinct ranges of model parameters (WTA: $\alpha = 1$ with large n; AVR: $\alpha = 0.5$ with $n = 1$). The *y*-axis represents the "pair" responses normalized by the responses to the max-location (pair/max) and the *x*-axis shows similarly normalized and summed responses to the two single locations [(max/max) + (min/max)] (Zoccolan et al. 2005). This latter calculation yields values between 1 (min = 0) and 2 (min = max), depending on the difference between the max- and min-responses for that pair of dots. The location of a data point in Fig. 5 is indicative for the spatial summation algorithm employed by the corresponding neuron (Fig. 5*A*) or pair condition (Fig. 5*B*) (Zoccolan et al. 2005). The larger black and white circles mark the two example neurons from Fig. 2, *A* and *B*, and Fig. 3, *A* and *B* (Fig. 5*A*) and their mean responses to 10 different pairs of locations (Fig. 5*B*). The scatter of data points with respect to the proposed summation algorithms is immediately apparent both across cells and across pair conditions for individual neurons. The spatial summation behavior ranges from pair responses being lower than the average of the component stimuli and thus close to the min-response (data points below the diagonal line) to pair responses being higher than the max-response and thus approaching linear summation (data points above the horizontal line). Yet again, the running median (black heavy line) computed along the abscissa (0.2 window shifted every 0.05) clearly shows that the population response to multiple stimuli closely resembles a WTA mechanism (Fig. 5*A*). The running median in Fig. 5*B* was calculated only for the pair conditions in which both locations yielded a significant response when stimulated individually (see METHODS). This approach limited the number of pairs with a WTA behavior that resulted from ineffectiveness of one of the composite stimuli (i.e., being placed outside the neuron's RF). Very similar results are obtained from the full data set. In addition, the scatter plots in Fig. 5 demonstrate that there is little dependence of the summation algorithm on the difference between the sensitivity of the component locations (the running median along the *x*-axis that lies consistently close to one).

Pair responses with attention. In addition to the fixation task, we trained monkey AT in a delayed match-to-sample task

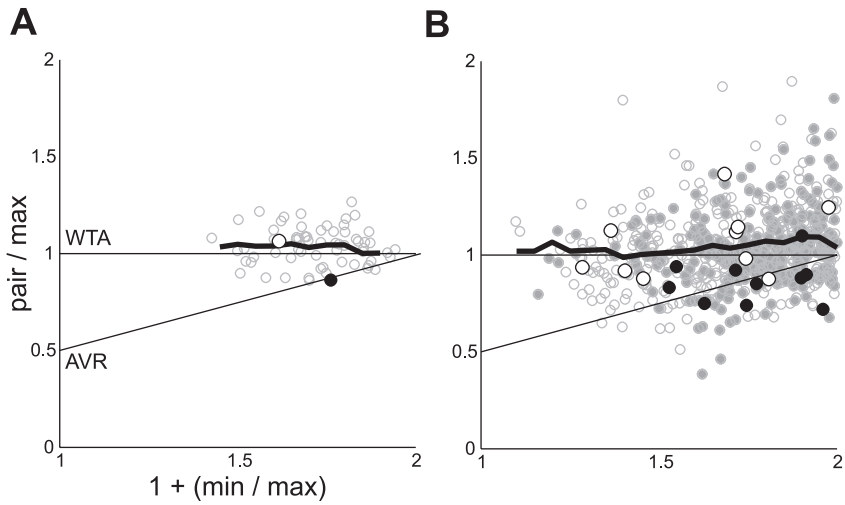

Fig. 5. *A* and *B:* comparison of the averaging (AVR) and winner-take-all (WTA) summation algorithms. Abscissa represents the sum of the responses to the 2 individually presented dots, normalized by the max-response (1 + min/max). Ordinates represent responses to a pair of simultaneously presented dots, normalized by the max-response (pair/max). *A*: average single neuron responses are plotted ($n = 64$) with the white and black dots marking the example neurons from Fig. 2, *A* and *B*, respectively. Heavy black line shows the running median calculated in a window with a width of 0.2 that was shifted in increments of 0.05. Lines labeled with WTA and AVR, respectively, indicate the values that are characteristic for WTA and AVR model. *B*: average responses for all tested pairs of dots (10 pairs per each neuron). Larger black and white circles mark the 10 pair conditions of the corresponding single units from *A*. Heavy black line represents the running median calculated across pairs for which both constituent locations evoked a significant single-stimulus response (filled grey circles).

(DMS), where it had to remember the locations of either a single dot or a pair of dots. We recorded responses of 17 single units during both tasks (the fixation data from these neurons were included in the previous analyses) and 31 neurons during the DMS task only. The DMS experiment allowed us to determine whether the cognitive state of the monkey affected the stimulus summation rule. More specifically, we compared the neuronal responses in conditions with attention directed away from the stimuli (the fixation task described earlier) with a task in which attention was evenly distributed across the targets (the DMS task). Visual stimulation in the two experiments was identical. Briefly, in the DMS task the animal was presented a sample stimulus (one or two dots) that after 0.5 s was followed by a variable delay period (0.7–1.0 s) and a test stimulus with the same number of dots as in the sample phase. To obtain a reward, the monkey had to lift its right hand when the location(s) were the same as in the sample phase (match) or its left hand when the sample and test location(s) differed (nonmatch). The monkey was given 2.5 s to give an answer, and when an answer was given, the test display was immediately terminated. Performance on this task differed between one-dot and two-dot trials, but it was high in both cases [mean percentage correct across 48 sessions, for one- and two-dot trials, respectively: 81 and 75%, $t(47) = 6.86$, $P < 0.01$; mean response times: 446 vs. 458 ms, $t(47) = 4.77$, $P < 0.01$]. In our analyses, we only used the neuronal responses from correctly completed trials.

To quantify the influence of attention on the spatial summation rule, we directly compared the neuronal responses from the 17 cells that provided data from both the fixation and the DMS experiments. On average, attentional demands were correlated with higher activity during the sample presentation compared with the fixation experiment, but the increase of firing rate was only significant for the single-dot trials, not for the pair responses [DMS vs. fixation for the pair condition: 73 vs. 62 spikes/s = 25% change, $t(16) = 1.8$, $P = 0.091$; max-location: 80 vs. 63 spikes/s = 36% change, $t(16) = 2.71$, $P = 0.015$; min-location: 80 vs. 63 spikes/s = 37% change, $t(16) = 3.17$, $P = 0.006$]. Since the ratio between the pair response and the max-response indicates how much the cells' normalization behavior resembles a WTA operation, we looked at the difference of this ratio between the DMS and fixation experiments. The mean pair-to-max ratio was 1.02 for the fixation task and 0.93 for the DMS task, which was a significant difference [$t(16) = 3.34$, $P = 0.004$; Fig. 6]. At the individual neuron level, this ratio was significantly greater in the fixation task for five of the neurons (29%, $P < 0.05$; Fig. 6). A similar comparison for the relative difference between the min- and max-responses (min/max) did not reach significance [$t(16) = 46$, $P > 0.6$].

The analysis of the population PSTH demonstrates that the difference between the fixation and DMS task in the normalization of the pair response is most prominent between ~200 and 300 ms after stimulus onset (Fig. 7, *A* and *C*). The black line in Fig. 7*A* that represents the mean pair response during the DMS task lies between the grey lines that mark the single-dot responses, an effect that is less obvious in Fig. 7*C* with the PSTHs from the fixation experiment. A more clear visualization of this notion is presented in Fig. 7*B* where the pair-to-max ratios for the DMS (dashed line) and the fixation (solid line) tasks are plotted as a function of sample presentation

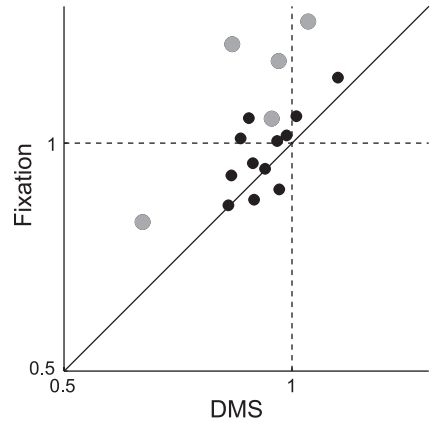

Fig. 6. Ratio of a pair response and a max-response for the delayed match-to-sample (DMS) and the fixation experiments. Seventeen single units from monkey AT recorded during both tasks. Thin dashed lines help to visualize how much the ratios in individual cells differ from a ratio of 1 (WTA behavior). Cells above the diagonal line have the pair-to-max ratio higher in the fixation than in the DMS experiment. Solid grey circles mark units with a significant difference between the tasks.

time (calculated in consecutive 40-ms wide bins). *P* values derived from *t*-tests that compare the ratios between the two experimental conditions for subsequent bins are shown in Fig. 7*D*.

Analogous PSTHs, calculated for the whole population of neurons from which we recorded during the DMS task ($n = 48$), further confirm the presence of an initial AVR phase followed by the WTA pair response (Fig. 8). Such temporally dynamic spatial summation behavior was observed for both the sample and the test phases of the DMS task (Fig. 8, *A* and *B*, respectively). The average duration of the test stimulus was shorter then the fixed 0.5-s sample presentation (mean response times across 48 sessions was 0.542 s with a minimum of 0.37 s). Interestingly, the shorter visual stimulation in the test phase of the DMS task was also reflected in the temporal profile of the pair responses, with the AVR phase being temporally compressed (Fig. 8*B*).

To further quantify the differences between the two attentional conditions and their possible influence on the spatial summation rule, we fitted the GSP model to describe the dot pair responses in relation to the activity evoked by the individual presentation of constituent dots. We directly compared the GSP model performance for the two experiments within a subgroup of 17 single units. The model fits for the fixation experiment are similar to the earlier analysis, which is not surprising since the 17 neurons used here for the comparison were selected from the full data set of 64 cells that were used before. The model explained 94% of sample pair-response variance with a best fitting scaling parameter near one ($\alpha = 0.97$, 95% CI: 0.88, 1.05). The power term was >1 ($n = 12$), but the CIs indicate that this estimate is not very reliable (95% CI: −55, 80). The DMS experiment fits yielded somewhat different parameters, but the percentage of sample stimulus response explained variance was very similar to that in the fixation task (94%). The best GSP model had scaling parameters of 0.5 (95% CI: −0.66, 1.67) and an n equal to 1 (95% CI: −2, 4).

The GSP model was also fit separately for the sample and the test phases of the DMS task on a single cell basis ($n = 48$, including 17 neurons that were also recorded during the fixation experiment). The time-averaged instantaneous spike rate

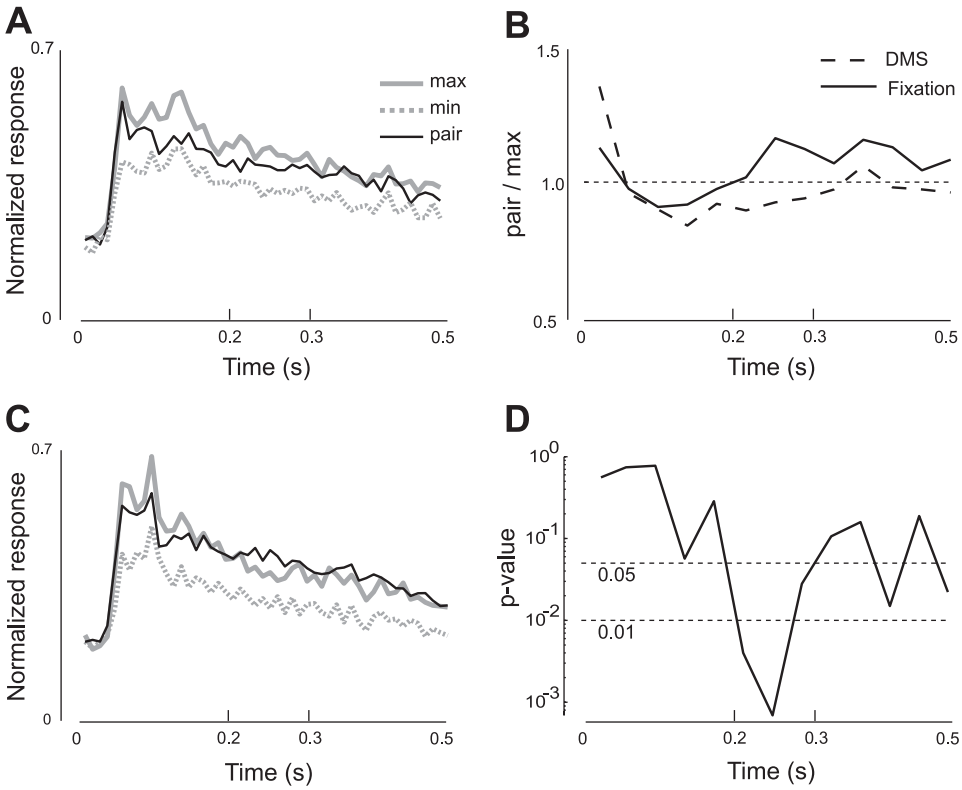

Fig. 7. Comparison of responses in the DMS and the fixation experiments. *A* and *C*: population PSTH (10-ms bins) from the DMS task (*A*) and the fixation task (*C*) with the data derived from the same 17 neurons. Conventions are the same as in Fig. 3*C*. *B*: pair-to-max ratio as a function of the sample presentation time for the DMS (dashed line) and the fixation (solid line) experiments. Mean ratio was calculated in 40-ms consecutive bins. First bin (from 1 to 40 ms of the sample onset) reflects an artifact related to a very low baseline activity in a number of cells and, consequently, unreasonably high values of the pair-to-max ratio. *D*: ratio from both tasks was compared for each of the bins and the *P* values obtained from the *t*-tests ($n = 17$) are plotted on a logarithmic scale.

for the test phase was adjusted to the response time since the test stimulus disappeared with the provided "match" or "nonmatch" answer. From a total of 48 units, the data from only 15 cells yielded a GSP model fit with an explained sample pair-response variance of >40% (Fig. 9*A*). The median scaling parameter for these 15 neurons was 0.81, whereas the exponent approached 2 (Fig. 9, *B* and *C*). The subset of cells for which each tested location evoked a significant sample response ($n = 12$) provided similar best-fit median parameter values ($\alpha = 0.78$ and $n = 1.7$). The visual responses of the test phase yielded slightly higher median best-fit parameters ($\alpha = 0.85$ and $n = 4.9$ for 16 out of 48 neurons with an explained variance >40%). Constraining the data set to the single units for which all probed locations yielded a significant test stimulus response resulted in the median parameters $\alpha = 0.88$ and $n = 5$. Taken together, the best GSP models for the fixation experiment tended to converge on the scaling parameters closer to one than the models that were fit to the DMS experiment data. However, in both cases the scaling is rather far from averaging.

DISCUSSION

In this study, we investigated how neurons in area 7a of the posterior parietal cortex encode pooled visual information across their receptive fields. We recorded from visual single units in the lateral bank of the IPS using very liberal sampling criteria to obtain a general description of the spatial summation algorithm for a population of parietal neurons. We measured responses elicited by stimulating either a single location or pairs of locations in the neuron's RF using identical small dots. The neuron's responses to pairs of dots were compared with the responses evoked by single dots, individually presented at the constituent locations. During a fixation task, the monkeys did not need to attend to the peripherally displayed dots, since no cognitive manipulation of any information with regard to these dots was required. The

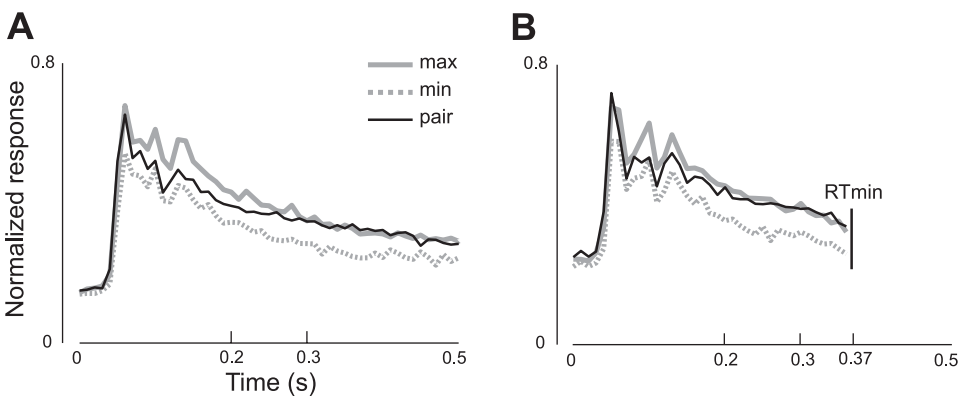

Fig. 8. *A* and *B*: temporal response profile for the sample (*A*) and the test (*B*) stimulus phases of the DMS task. Unsmoothed population PSTH ($n = 48$) with normalized responses. Conventions are the same as in Fig. 3.

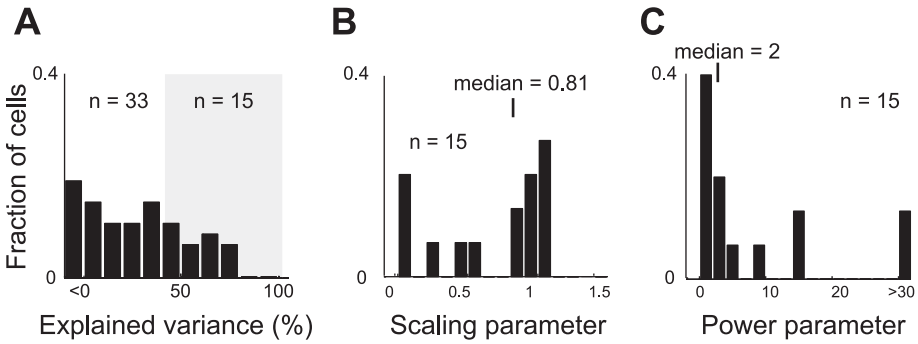

Fig. 9. GSP model fits for the sample phase of the DMS experiment. *A*: results of model fitting for 48 neurons expressed as the percentage of the explained variance accounted for by the model. *B*: distribution of the best-fit scaling parameter α from single units for which the best fitting model explained ≥40% of the sample pair-response variance ($n = 15$). *C*: same as in *B* but for the power parameter n.

results of the fixation experiment were very clear at the population level. Irrespective of a considerable scatter of data points between and within neurons, various analyses indicated the presence of a clear WTA operation. Average responses to a pair of dots very closely resembled the response evoked by the stimulus that gave the largest response when it was presented in isolation. Such results are in contrast with most of the literature in which AVR algorithms are reported for equivalent conditions (Miller et al. 1993; van Wezel et al. 1996; Luck et al. 1997; Recanzone et al. 1997; Britten and Heuer 1999; Reynolds et al. 1999; Zoccolan et al. 2005; Busse et al. 2009). The GSP model (Britten and Heuer 1999; Simoncelli and Heeger 1998) fitted to the data from paired presentations demonstrated little scaling and an appreciable nonlinearity that correlates with WTA behavior. However, it must be noted that the GSP model could not reliably explain the pair-response variance for >40% of the neurons that were recorded with the fixation task. While the overall variability of the summation rule across neurons and visual conditions might partially result from a low signal-to-noise ratio of the recording technique, it is also very likely that the individual parietal neurons are rather noisy encoders themselves. The latter explanation stresses the possible importance of a gain control mechanism in the cortical network that achieves a near perfect WTA spatial integration from the many noisy responses of the individual neurons in the population.

With a control experiment in which a monkey performed a delayed match-to-sample task, we tested whether the distribution of attention over space had any effect on the spatial summation mechanism. We directly compared the responses of single neurons during the fixation task with minimal attention on the stimulus dots to the responses during the DMS task that explicitly required attention directed to the two concurrently present dots. Basically, these responses were shown to be enhanced when attention is directed towards the stimuli in the RF. Interestingly, this effect was much larger in the single-dot conditions than in the paired dot responses, for which the two tasks were not significantly different. This unequal attentional modulation that depended on the number of attended stimuli resulted in max-to-pair-response ratios that were lower for the DMS task than for the fixation task (even though the ratios on both tasks were close to unity).

The ultimate effect of attention in the current experiments was manifested in a shift of the WTA behavior towards an AVR rule. One of the concerns with this interpretation is that the magnitudes of the pair responses in the DMS experiment were at the upper limit of the neurons' response range. However, inspection of the temporal dynamics of neuronal activation suggests that the greatest difference between the attentional contexts was present between 200 and 300 ms after stimulus onset and that this is phase of the response at which the firing rate is much lower than at the early transient peak (Fig. 7). The comparison of Fig. 3*C* and Fig. 8*A* with a larger number of recorded neurons (64 from the fixation and 48 from the DMS tasks) accentuates the difference in the temporal profile of the pair responses that we quantified with a series of *t*-tests for the subgroup of cells recorded in both experiments ($n = 17$). Thus there is more averaging during integration of stimuli across the RF when attentional resources are applied than when the monkey performs a simple fixation task. Still, the last 200 ms of the multiple stimulus presentation for both the fixation and the DMS tasks bear the signature of a WTA algorithm.

One of the interpretations of the differences between the fixation and the DMS tasks advocates a possible difference in response tuning for distinct cognitive processes (Crowe et al. 2004). However, due to the similarity of the two tasks in terms of visual stimulation and the mode of response, we favor a different and more parsimonious explanation. We suggest that the representation of the min-stimulus gains strength through attentional magnification and thereby becomes a stronger opponent in the neuronal competition. In Fig. 3*C*, the peak of the min-response is somewhat shifted from both the stimulus onset and the peak of the max-response. This particular modulation of timing might facilitate a WTA operation. Even as the min-response has a similar response onset, the delayed peak could be easily suppressed by the max-response. Such temporal gating mechanism was previously proposed by Gawne (2008) to explain the max-behavior of some V4 neurons (Gawne and Martin 2002). Further exploration of this interesting potential mechanism requires more extensive investigation with larger neuronal pools.

Our fixation experiment demonstrated that, over the population of area 7a neurons, a WTA mechanism is the default computational rule to spatially integrate visual information across the RF. In this experiment, the min-stimulus does not get any additional attentional boost and it can therefore not compete for neuronal representation with the concurrently presented max-stimulus. Metaphorically, without attention, the "loser" gives up the battle pretty quickly. Extending this figure of speech, when both stimuli benefit from attentional gain, the loser will compete for neuronal representation until it eventually (and unavoidably) has to give way to the max-stimulus.

To summarize, in this study we assessed the spatial summation algorithm employed by neurons in the posterior parietal cortex. Notwithstanding the remarkable amount of research

interest PPC has received in the context of the control of spatial attention (Steinmetz and Constantinidis 1995; Gottlieb et al. 1998; Colby and Goldberg 1999; Constantinidis and Steinmetz 2001, 2005; Corbetta and Shulman 2002; Bisley and Goldberg 2003, 2006; Constantinidis 2006), we are the first to show how single cells in this brain area pool visual information across their receptive fields. Our results bear important implications for attention models of single-unit responses in the parietal cortex (cf., Ghose and Maunsell 2008; Ghose 2009). The competitive interactions between multiple stimuli within the RF of a PPC neuron are won by the more optimal of two simultaneously presented visual objects, demonstrating a WTA summation algorithm. However, when attention is directed towards these stimuli the winner phase of the response to such a pair of stimuli is shifted towards an AVR algorithm. The demonstrated max-behavior of area 7a neurons, which turned out to be irrespective of attention, could reflect this brain region's role in the integration of bottom-up attention for salient stimuli (Constantinidis and Steinmetz 2001, 2005).

ACKNOWLEDGMENTS

We thank Jacob Duijnhouwer for assistance with the custom-made software and Theo Stuivenberg, Erik Aarnoutse, Ed van der Veen, and Hans Borgeld for technical support.

GRANTS

This study was supported by a grant of the Netherlands Organisation for Scientific Research (NOW; Evolution and Behaviour: 051-14-027).

DISCLOSURES

No conflicts of interest, financial or otherwise, are declared by the author(s).

REFERENCES

Bisley JW, Goldberg ME. Neuronal activity in the lateral intraparietal area and spatial attention. *Science* 299: 81–86, 2003.

Bisley JW, Goldberg ME. Neural correlates of attention and distractibility in the lateral intraparietal area. *J Neurophysiol* 95: 1696–1717, 2006.

Britten KH, Heuer HW. Spatial summation in the receptive fields of MT neurons. *J Neurosci* 19: 5074–5084, 1999.

Busse L, Wade AR, Carandini M. Representation of concurrent stimuli by population activity in visual cortex. *Neuron* 64: 931–942, 2009.

Carandini M, Heeger DJ, Movshon JA. Linearity and normalization in simple cells of the macaque primary visual cortex. *J Neurosci* 17: 8621-8644, 1997.

Colby CL, Goldberg ME. Space and attention in parietal cortex. *Annu Rev Neurosci* 22: 319–349, 1999.

Constantinidis C. Posterior parietal mechanisms of visual attention. *Rev Neurosci* 17: 415–427, 2006.

Constantinidis C, Steinmetz MA. Neuronal responses in area 7a to multiple-stimulus displays. I. neurons encode the location of the salient stimulus. *Cereb Cortex* 11: 581–591, 2001.

Constantinidis C, Steinmetz MA. Posterior parietal cortex automatically encodes the location of salient stimuli. *J Neurosci* 25: 233–238, 2005.

Corbetta M, Shulman GL. Control of goal-directed and stimulus-driven attention in the brain. *Nat Rev Neurosci* 3: 201–215, 2002.

Crowe DA, Chafee MV, Averbeck BB, Georgopoulos AP. Neural activity in primate parietal area 7a related to spatial analysis of visual mazes. *Cereb Cortex* 14: 23–34, 2004.

Finn IM, Ferster D. Computational diversity in complex cells of cat primary visual cortex. *J Neurosci* 27: 9638–9648, 2007.

Gawne TJ. Stimulus selection via differential response latencies in visual cortical area V4. *Neurosci Lett* 435: 198–203, 2008.

Gawne TJ, Martin JM. Responses of primate visual cortical V4 neurons to simultaneously presented stimuli. *J Neurophysiol* 88: 1128–1135, 2002.

Ghose GM. Attentional modulation of visual responses by flexible input gain. *J Neurophysiol* 101: 2089–2106, 2009.

Ghose GM, Maunsell JH. Spatial summation can explain the attentional modulation of neuronal responses to multiple stimuli in area v4. *J Neurosci* 28: 5115–5126, 2008.

Gottlieb JP, Kusunoki M, Goldberg ME. The representation of visual salience in monkey parietal cortex. *Nature* 391: 481–484, 1998.

Ipata AE, Gee AL, Bisley JW, Goldberg ME. Neurons in the lateral intraparietal area create a priority map by the combination of disparate signals. *Exp Brain Res* 192: 479–488, 2009.

Kusunoki M, Gottlieb J, Goldberg ME. The lateral intraparietal area as a salience map: the representation of abrupt onset, stimulus motion, and task relevance. *Vision Res* 40: 1459–1468, 2000.

Lampl I, Ferster D, Poggio T, Riesenhuber M. Intracellular measurements of spatial integration and the max operation in complex cells of the cat primary visual cortex. *J Neurophysiol* 92: 2704–2713, 2004.

Lee J, Maunsell JH. A normalization model of attentional modulation of single unit responses. *PLos One* 4: e4651, 2009.

Luck SJ, Chelazzi L, Hillyard SA, Desimone R. Neural mechanisms of spatial selective attention in areas V1, V2, and V4 of macaque visual cortex. *J Neurophysiol* 77: 24–42, 1997.

Miller EK, Gochin PM, Gross CG. Suppression of visual responses of neurons in inferior temporal cortex of the awake macaque by addition of a second stimulus. *Brain Res* 616: 25–29, 1993.

Moran J, Desimone R. Selective attention gates visual processing in the extrastriate cortex. *Science* 229: 782–784, 1985.

Recanzone GH, Wurtz RH, Schwarz U. Responses of MT and MST neurons to one and two moving objects in the receptive field. *J Neurophysiol* 78: 2904–2915, 1997.

Reynolds JH, Chelazzi L, Desimone R. Competitive mechanisms subserve attention in macaque areas V2 and V4. *J Neurosci* 19: 1736–1753 1999.

Reynolds JH, Heeger DJ. The normalization model of attention. *Neuron* 61: 168–185, 2009.

Simoncelli EP, Heeger DJ. A model of neuronal responses in visual area MT. *Vision Res* 38: 743–761, 1998.

Steinmetz MA, Constantinidis C. Neurophysiological evidence for a role of posterior parietal cortex in redirecting visual attention. *Cereb Cortex* 5: 448–456, 1995.

van Wezel RJ, Lankheet MJ, Verstraten FA, Maree AF, van de Grind WA. Responses of complex cells in area 17 of the cat to bi-vectorial transparent motion. *Vision Res* 36: 2805–2813, 1996.

Zoccolan D, Cox DD, DiCarlo JJ. Multiple object response normalization in monkey inferotemporal cortex. *J Neurosci* 25: 8150–8164, 2005.